JOURNAL OF MATERIALS SCIENCE 37 (2002) 3903–3913

Crystallographic structure of gold films electrodeposited at low current densities

B. BOZZINI*
INFM, Dipartimento di Ingegneria dell'Innovazione, Università di Lecce, v. Monteroni, I-73100 Lecce, Italy
E-mail: Benedetto.Bozzini@unile.it

G. GIOVANNELLI, S. NATALI
Dipartimento ICMMPM, Università di Roma 1, v. Eudossiana 18, I-00184 Roma, Italy

A. FANIGLIULO
INFM, Dipartimento di Ingegneria dell'Innovazione, Università di Lecce, v. Monteroni, I-73100 Lecce, Italy

P. L. CAVALLOTTI
Dipartimento di Chimica Fisica Applicata, Politecnico di Milano, v. Mancinelli 7, I-20131 Milano, Italy

In this paper we report on the electrodeposition of Au from dicyanoaurate electrolytes at low current densities. If electrodeposition is carried out at current densities lower than 0.25 mA cm^{-2} a new hexagonal crystalline structure can be observed. This structure is generally codeposited with fcc Au. The new structure dominates for short deposition times. This structure is stabilised by the addition to the bath of metal ions giving rise to UPD behaviour on Au, such as Cu^{2+} and Tl^{+}. This structure was tentatively assigned to the space group 184 (p6cc). This structure can be explained in terms of the incorporation of extraneous, probably cyanide-related, material. This interpretation is also supported by *in situ* Raman spectroscopy and by XPS analyses showing that the bulk deposits contain C, N and K. The electrochemical behaviour of the electrodeposition system was studied by cyclic voltammetry. Cyanoaurate baths display a significant cathodic passivation. This phenomenon is reduced by the addition of Cu^{2+} or Tl^{+}. Voltammograms of baths containing these additives show clear UPD features but no stripping peaks. This behaviour is suggestive of an assisted Au electrodeposition mechanism. Tl is deposited at UPD and oxidatively desorbed by Au(I). Cu is codeposited at UPD with Au forming an alloy.

1. Introduction

Electrodeposition of Au and Au alloys for applications in jewellery amounts to ca. 6% of the overall amount of electrodeposited Au world-wide. The plating is carried out mostly with cyanoalkaline solutions containing free cyanide. Use of near netural dicyanoaurate baths not containing free cyanide is gaining momentum for obvious reasons, but the industrial acceptance of these solutions is still limited by difficulties in controlling the plating process. This state of affairs calls for fundamental understanding of the electrodic kinetics and related structural and compositional effects. In particular electroforming holds an appreciable share (ca. 40%) of the global amount of Au electrodeposited for jewellery applications. This electrochemical technique displays considerable competitive advantages against microcasting in the low-cost (<500 USD) jewels niche, nevertheless major technical problems with the state-of-the-art processes are hindering this tendency. As far as Au-alloy electroforming is concerned, three kinds of processes were proposed in the past: free-cyanide Au-Cu [1], free-cyanide Au-Cu-Cd [2] and low-cyanide Au-Ag [3]. In the past, the only industrially feasible process proved the Au-Cu-Cd one, the other two methods giving rise to unacceptable compositional variations, irreproducible crystalline structures and uncontrolled mechanical properties. The Au-Cu-Cd process is nevertheless affected by serious drawbacks, the most severe ones being time-dependent brittleness and space- and time-dependent compositional variations. In addition, high concentrations of free cyanide are required for the operation of the bath and 4–7% of Cd is present in the product, leading to health hazard in soldering and possible allergy problems for end users.

Much research was devoted by a group of Italian universities in understanding the electrochemical

*Author to whom all correspondence should be addressed.

problems of Au and Au-alloy electrodeposition, and they proposed industrially viable alternatives (see e.g., [4]). Most of the mechanical problems were explained by hydrogen embrittlement, and the electrochemical effects of Cd^{2+} additions were interpreted in terms of specific electrokinetic effects [5, 6]. The proposal ensued of a Au-Cu electroforming process based on Cu^{2+}-EDTA complexes and not containing free-cyanide. The process yields very reproducible and easily controllable composition, hydrogen embrittlement problems—though still present—are well understood and can be technically dominated without resorting to empirical approaches. Further research was carried out to try to eliminate hydrogen inclusion and to understand the electrochemical reasons for the traditional use of thallium and arsenic additions to Au plating baths.

In this paper we report on peculiarities related to the crystalline structures which are observed when plating at low current densities (c.d.) from slightly acidic dicyanoaurate solutions. These crystalline structures are most probably related to the incorporation of extraneous, cyanide-related material. The structural investigation is complemented by voltammetric, *in situ* Raman and XPS analyses. Preliminary information on the mechanical and electronic properties of these systems is also provided.

2. Experimental

The basic bath composition and operating conditions were: $KAu(CN)_2$ 12 $g\,l^{-1}$, citric acid 40 $g\,l^{-1}$, NH_4^+-citrate 40 $g\,l^{-1}$, room temperature, unstirred. The anodic to cathodic surface area ratio was larger than 10. Cathodic substrates were: laminated Cu (with a very weak (111) XRD peak), annealed Cu, X-ray amorphous Ni-P (9%), annealed Mond Ni. Additives to the basic bath were: $TlNO_3$ 40 ppm, Cu(II)-EDTA 2.5 $g\,l^{-1}$.

Cyclic voltammograms (CV) were measured in solutions containing the same citrate buffer and the metals diluted by a factor of 20 with respect to the electrodeposition baths at a scan rate of 1 V s^{-1}. The WE was polycrystalline Au wire, the CE was a platinised expanded mesh Ti electrode, the RE was SCE.

X-ray diffraction (XRD) measurements were carried out with Cu radiation and a thin film goniometer. XPS analyses were performed with Al radiation and a HSA analyser. Recording hardness measurements (RHM) were carried out with a load of 10 mN applied for 10 s. Electrical conductivity measurements were carried out with a four-point device operated at a frequency of 480 kHz. *In situ* Raman spectroscopy measurements were carried out with a LabRam true confocal spectrometer and He-Ne radiation.

3. Results and discussion

3.1. Crystallographic structure as a function of electrodeposition conditions

3.1.1. Au electrodeposition in presence of Cu^{2+} or Tl^+ in the c.d. range 0–0.250 mA cm^{-2}

Two-phase deposits are obtained containing: (i) a new structure (hence NS) and (ii) fcc Au. The amount of the fcc Au phase tends to increase with electrodeposition time: below ca. 200 atomic layers the NS is the dominating phase (Fig. 1), above 0.2 μm (deposition times in

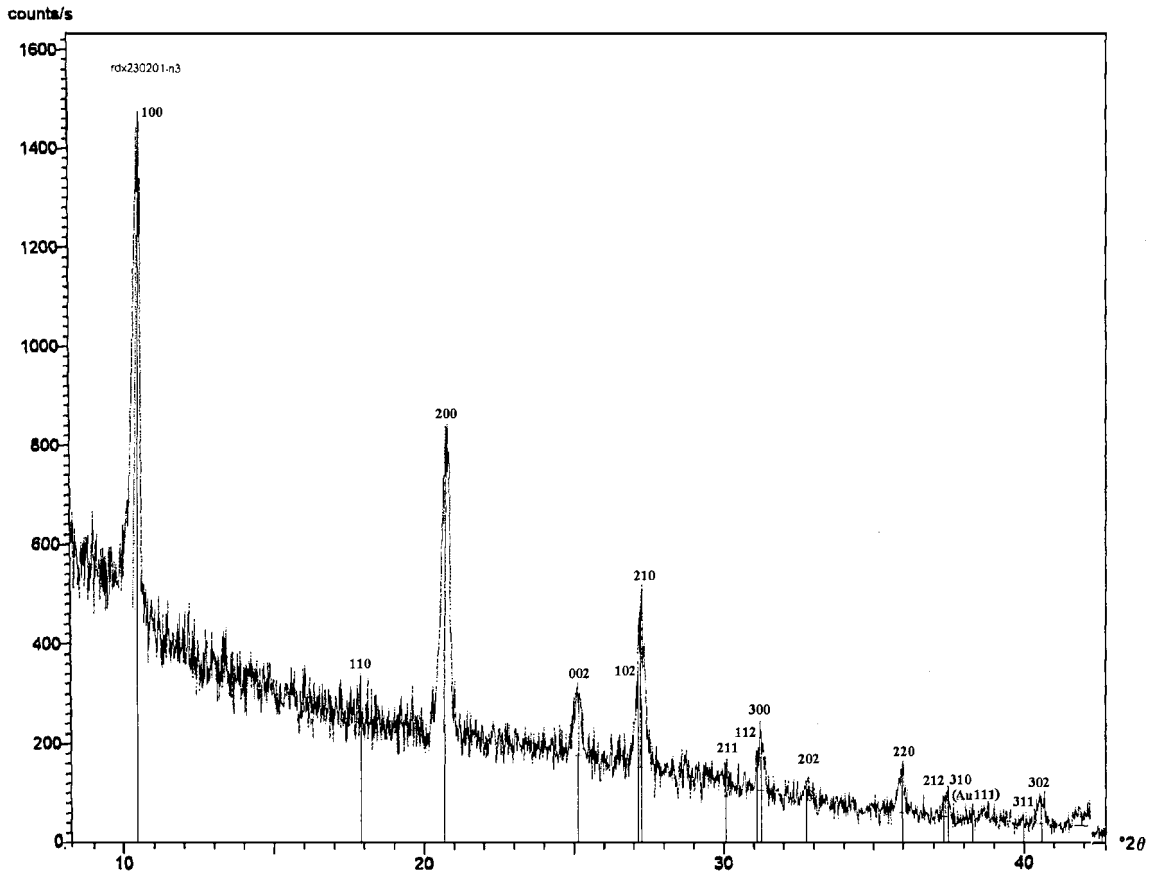

Figure 1 X-ray diffractogram of Au electrodeposited on annealed Cu at 0.125 mA cm^{-2} for 90 s from a bath containing 40 ppm Tl^+—new structure NS and traces of fcc Au.

excess of 1 h) the fcc Au prevails. One can assume that if the electrodeposition time is extrapolated to zero, the amount of fcc Au tends to vanish. It is worth observing that a Au displacement layer obtained at room temperature cannot be detected with the grazing-angle XRD equipment available for this research, while a marked fcc Au (111) can be observed if the Cu substrate is immersed in the plating bath at 40°C.

Estimates of the time evolution of the preferred orientation (PO) (expressed as the ratio of peak heights I_{010}/I_{120}) of the NS and of the NS to Au phase content (expressed as ratio of peak heights $I_{010}/I_{\mathrm{Au}(111)}$) are reported in Tables I and II. It can be observed that the relative amount of fcc Au to NS tends to grow and that the preferred orientation of the NS tends to change from (010) to (120) as the sample thickness grows. The type of crystallinity of the deposits is not markedly affected by electrodeposition time. In the case of [Tl^+] 40 ppm and c.d. 0.125 mA cm^{-2}, both NS and Au show typical crystallite dimensions around 23 nm (estimated by the Scherrer method on the NS (101) and Au (111) peaks). In the case of [Cu^{2+}] 2.5 g l^{-1} and c.d. 0.25 mA cm^{-2}, both NS and Au show typical crystallite dimensions of about 23 and 15 nm, respectively.

TABLE I Preferred orientation of the new structure NS (I_{010}/I_{120}) and phase content of NS and fcc Au ($I_{010}/I_{\mathrm{Au}(111)}$) as a function of electrodeposition time for [Tl^+] 40 ppm and c.d. 0.125 mA cm^{-2}

t (s)	90	240	360	3600
I_{010}/I_{120}	2.94	5.83	1.48	1.05
$I_{010}/I_{\mathrm{Au}(111)}$	97.0	13.4	5.18	0.574

TABLE II Preferred orientation of the new structure NS (I_{010}/I_{120}) and phase content of NS and fcc Au ($I_{010}/I_{\mathrm{Au}(111)}$) as a function of electrodeposition time for [Cu^{2+}] 2.5 g l^{-1} and c.d. 0.250 mA cm^{-2}

t (s)	120	600	900	3600
I_{010}/I_{120}	8.24	0.949	0.426	0.311
$I_{010}/I_{\mathrm{Au}(111)}$	31.8	0.597	0.734	0.014

3.1.2. Au electrodeposition in presence of Cu^{2+} or Tl^+ for c.d. >0.250 mA cm^{-2}

In these conditions the fcc Au phase becomes the dominating one, even for short electrodeposition times. In these conditions addition of Cu^{2+} to the bath gives rise to the formation of a substitutional fcc solid solution. The relevant diffractograms display peak shifts coherent with the Végard law (Fig. 2). In this c.d. range addition of Tl^+ brings about the formation of a three-phase structure: (i) NS, (ii) fcc Au without Végard shift, (iii) reflections which can be indexed with reference to the species AuCN (see below), which—in principle—could be mechanically incorporated (Fig. 3).

3.1.3. Au electrodeposition in presence of Cu^{2+} or Tl^+ for c.d. >1 mA cm^{-2}

Under these operating conditions, the NS can no longer be observed. The phase composition shows: (i) fcc Au, (ii) metastable hydrides (7) with a very evident sharp peak at $d = 4.9930$ Å, which disappears if the sample is stored at room temperature for times typically in excess of 10 h (Fig. 4).

3.1.4. Au electrodeposition from solutions not containing additives

Electroplating in these baths is characterised by a marked cathodic passivation. The progress of this passivating behaviour can be mesured e.g., by cyclic voltammetry, by monitoring the electrode potential required to achieve a given c.d. level as cycling at a high scan rate (minimising effects of mass transport) progresses (Fig. 5). X-ray diffractograms measured under these conditions are poorly reproducible, but typically show

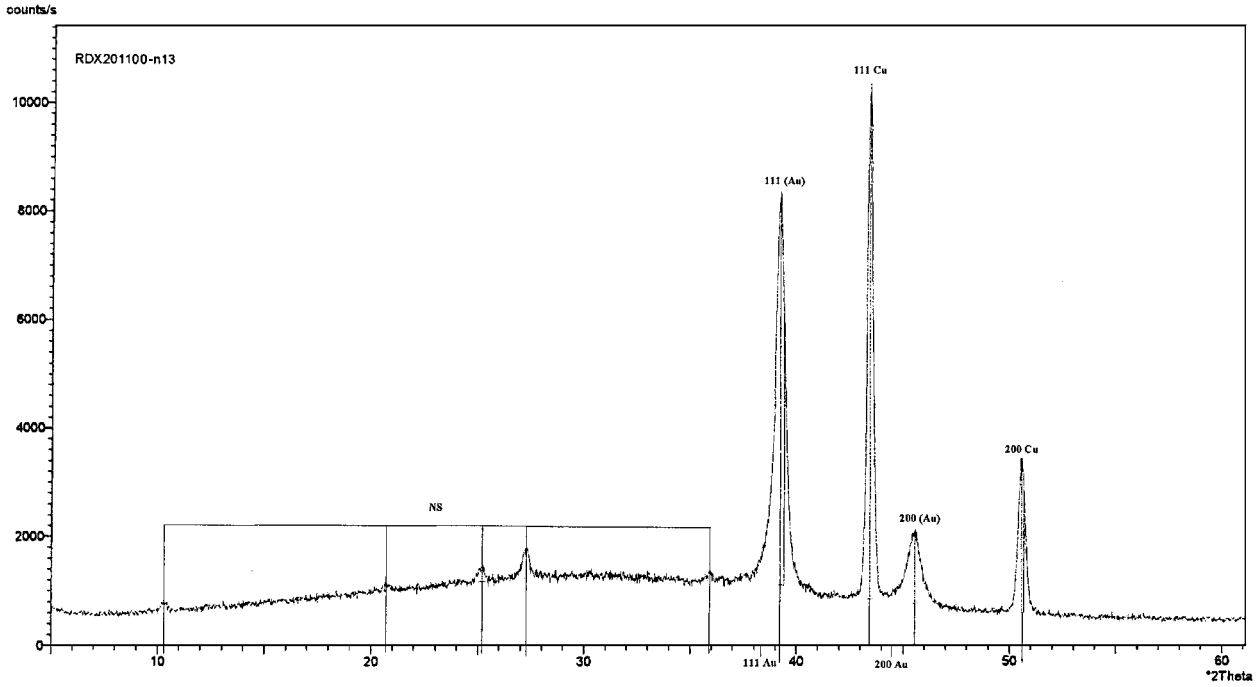

Figure 2 X-ray diffractogram of Au electrodeposited on annealed Cu at 0.5 mA cm^{-2} for 300 s from a bath containing 2.5 g l^{-1} Cu(II)-EDTA—fcc Au (with Végard peak shift) and traces of the new structure NS.

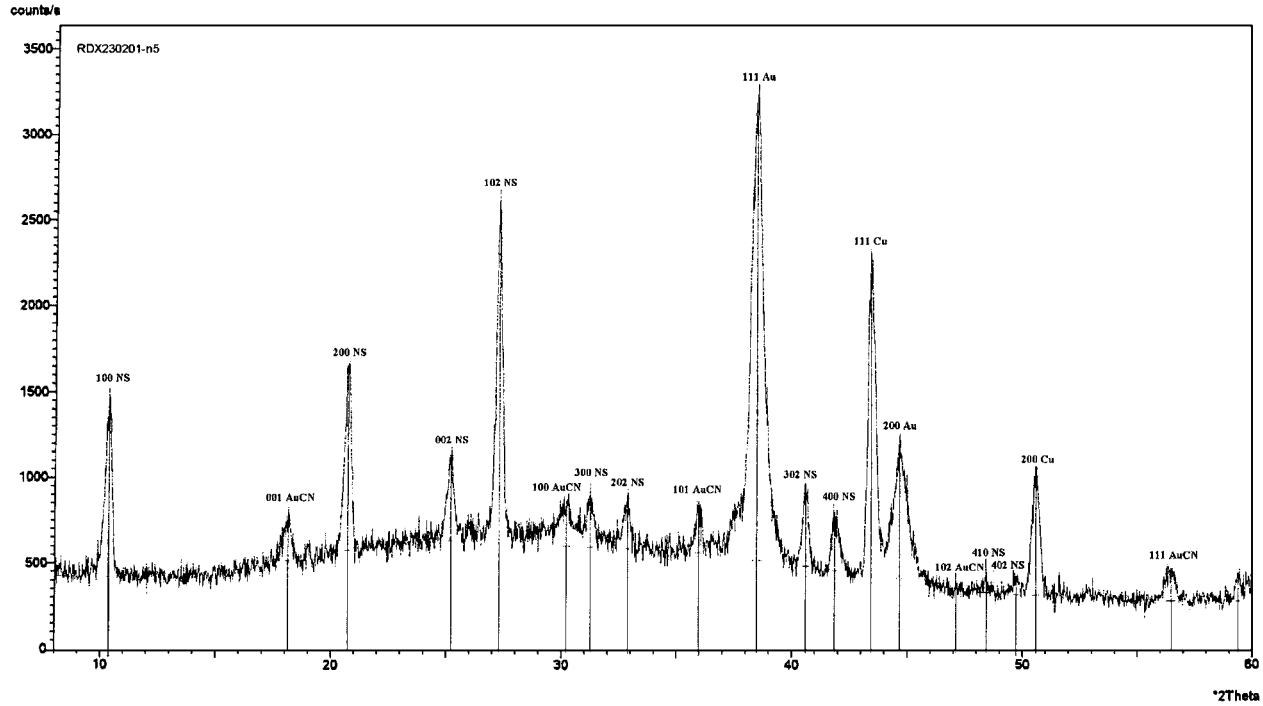

Figure 3 X-ray diffractogram of Au electrodeposited on annealed Cu at 0.5 mA cm^{-2} for 180 s from a bath containing 40 ppm Tl^{+}—(i) new structure NS, (ii) fcc Au (without Végard peak shift), (iii) reflections which can be indexed as AuCN.

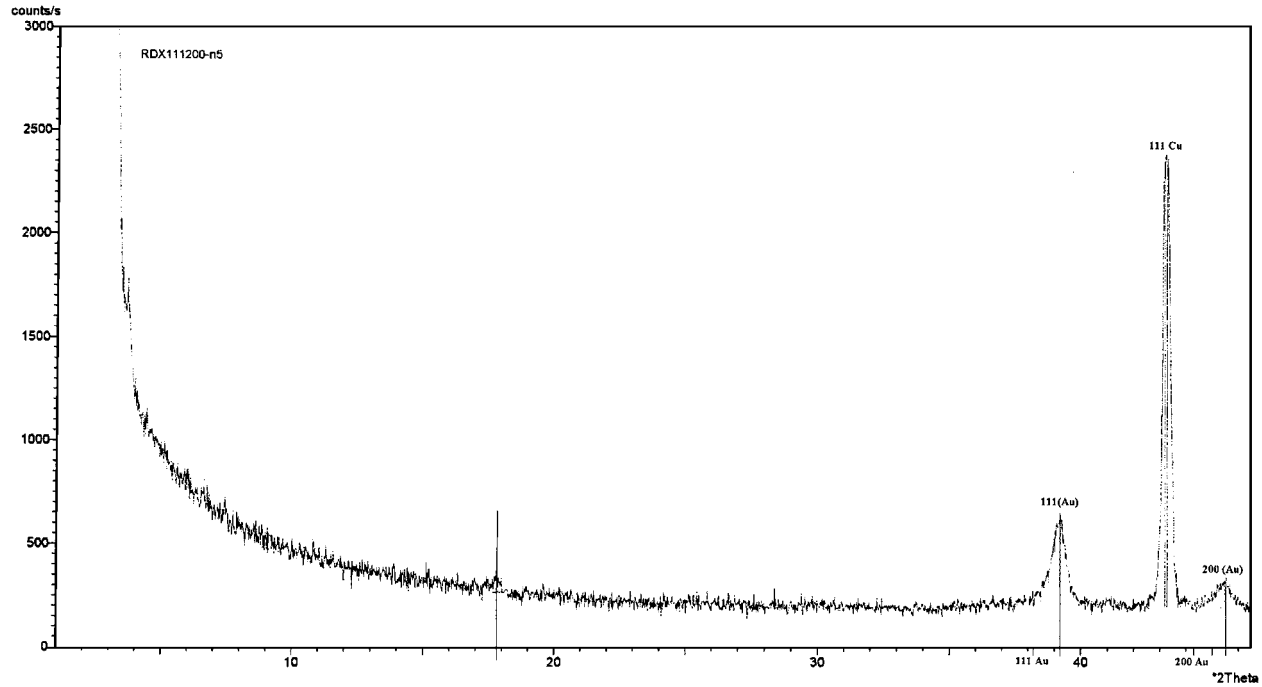

Figure 4 X-ray diffractogram of Au electrodeposited on annealed Cu at 1.0 mA cm^{-2} for 150 s from a bath containing 2.5 g l^{-1} Cu(II)-EDTA—(i) fcc Au, (ii) traces of metastable hydrides.

the following phase composition. (i) For short deposition times (120 ÷ 240 s) a two—phase structure appears displaying weak reflections—which can be explained with the NS—, together with fcc Au reflections (Fig. 6). (ii) After prolonged electrodeposition (720÷3600 s) the NS can no longer be observed while fcc Au dominates; some further peaks can be noticed which are very close to—though they do not coincide with—those of AuCN (space group 183 (P6mm), $a = 3.3395$ Å, $c = 1.4963$ Å) (Figs 7, 8). It is worth noticing that in these conditions the peak at ca. 18° 2θ vanishes in 3 h after completion of the electrodeposition process. Preliminary SAED data of the uppermost region of the deposit show reflections which can be indexed with the AuCN structure. The presence of the NS in experiments carried out in baths not containing additives and the limited reproducibility of the crystallographic structures obtained in these conditions can be tentatively explained with the presence of traces of metals giving UPD behaviour on Au (e.g., Ag, a typical impurity contained in $KAu(CN)_2$).

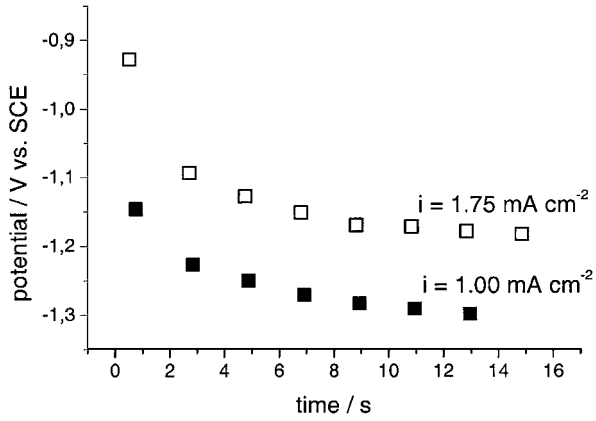

Figure 5 Cathodic potentials at constant current densities from cyclic voltammetric measurements.

3.2. Crystallographic effects of additive, electrodeposition time, nature of the substrate, heat-treatments and ageing

Diffractograms measured on Au layers deposited onto: (i) X-ray amorphous Ni-P (P 9%), (ii) annealed and wrought Cu, (iii) annealed Ni together with the ones mentioned prieviously, show the following common features (see, e.g., Fig. 9). (i) A marked independence of the peak positions and intensities on the nature of the employed additive. (ii) Reduction of the hhh type intensities and increase of the 00k ones with deposition time. (iii) A very limited dependence of the relative intensities on: (a) chemical nature, (b) crystalline or amorphous state as well as on the annealed or strained state of the substrate. The NS is markedly stable against

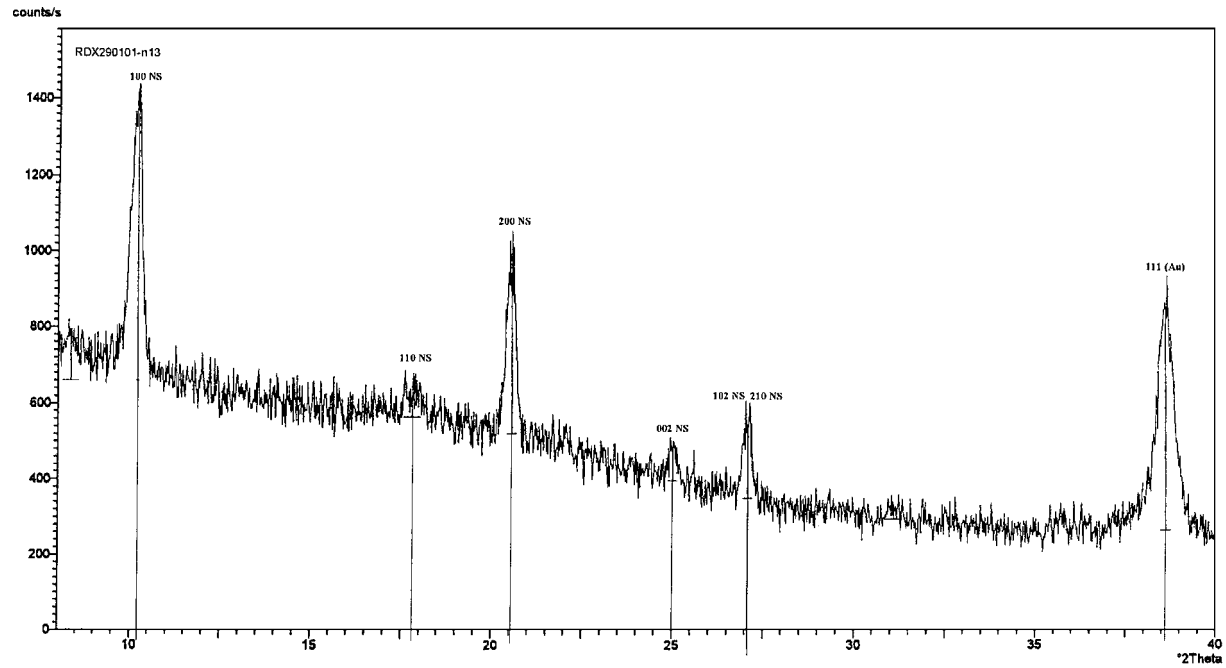

Figure 6 X-ray diffractogram of Au electrodeposited on wrought Cu at 0.125 mA cm^{-2} for 240 s from a bath not containing additives—(i) new structure NS, (ii) fcc Au.

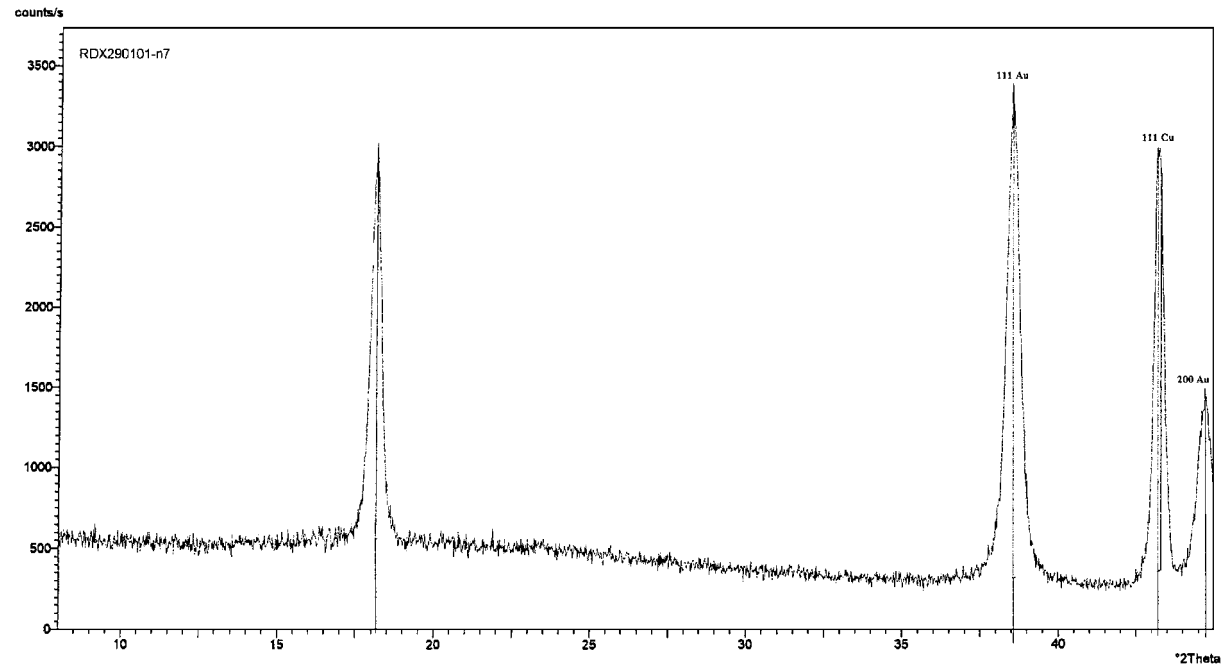

Figure 7 X-ray diffractogram of Au electrodeposited on wrought Cu at 0.125 mA cm^{-2} for 720 s from a bath not containing additives—(i) fcc Au, (ii) space group 183 (similar to AuCN).

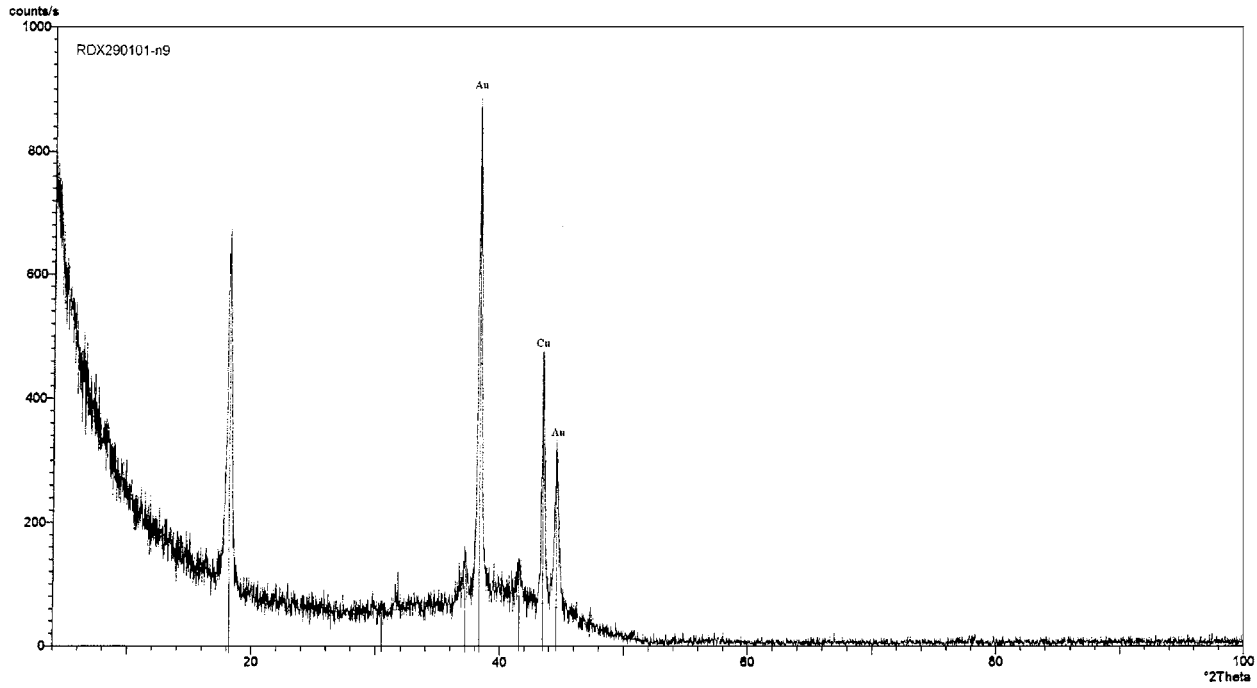

Figure 8 X-ray diffractogram of Au electrodeposited on wrought Cu at 0.25 mA cm^{-2} for 3600 s from a bath not containing additives—(i) fcc Au, (ii) space group 183 (similar to AuCN).

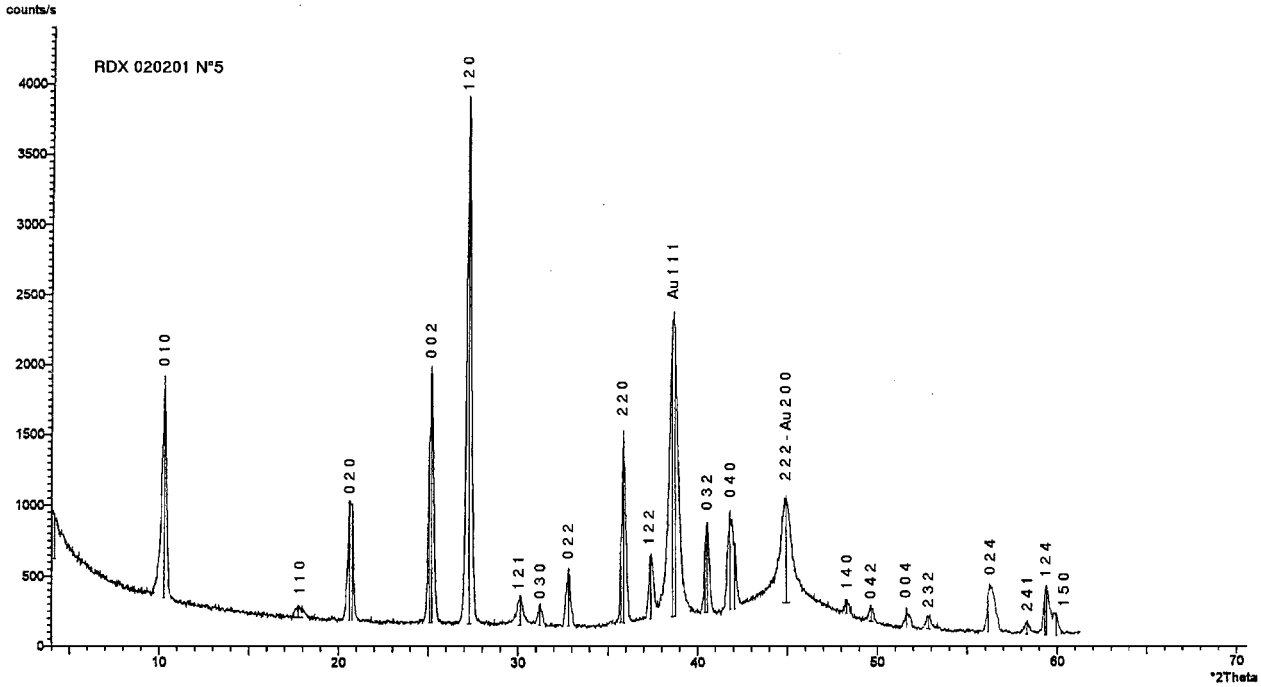

Figure 9 X-ray diffractogram of Au electrodeposited on X-ray amorphous Ni-P (P 9%) at 0.25 mA cm^{-2} for 900 s from a bath containing 2.5 g l^{-1} Cu(II)-EDTA—(i) new structure NS, (ii) fcc Au.

isothermal heat-treatments carried out at ∼100°C for ∼1 h. More thorough investigations of the thermal stability of this phase are in order. As far as temporal stability is concerned, diffractograms replicated after 6 months are identical.

Concerning crystallite dimensions, it can be noticed that the fcc Au phase tends to grow more nanocrystalline as c.d. increases. A general approximate trend, which can be observed both with and without presence of additives and in structures with different phase compositions is the following: 0.125–0.25 mA cm^{-2}, ∼24 nm; 0.5 mA cm^{-2}, ∼13 nm; 1 mA cm^{-2}, ∼11 nm.

3.3. Chemical analyses

Compositional analyses of samples deposited from a AuCu bath at 0.125 mA cm^{-2} were performed by XPS. Survey spectra for unsputtered surfaces (Fig. 10) display a significant enrichment in oxidised Cu(II) ($2p_{3/2}$ 933.0 eV) only traces of oxidised Au ($4f_{7/2}$ 86.3 eV) are present. A large adventitious carbon peak (1s 284.6 eV) is of course observed on the unsputtered surface.

XPS survey spectra obtained from the bulk of the deposit after extensive Ar^+ sputtering (Fig. 11) show the following peaks: Au(0) ($4f_{7/2}$ 84.6 eV), oxidised Au ($4f_{7/2}$ 85.8 eV) with an atomic ratio

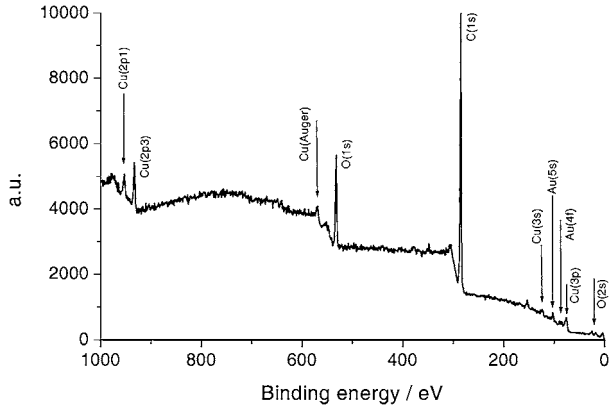

Figure 10 XPS survey spectrum of unsputtered surface of obtained by electrodepositing at 0.125 mA cm^{-2} for 300 s from a bath containing 2.5 $g\,l^{-1}$ Cu(II)-EDTA.

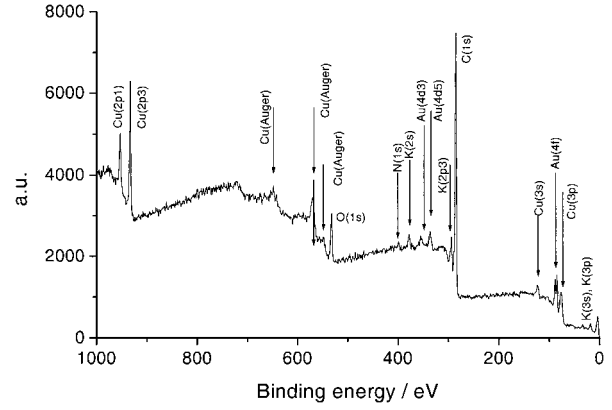

Figure 11 XPS survey spectrum of Ar^{+}-sputtered surface obtained by electrodepositing at 0.125 mA cm^{-2} for 300 s from a bath containing 2.5 $g\,l^{-1}$ Cu(II)-EDTA.

Au(0)/Au(ox) = 2.7, Cu(0) ($2p_{3/2}$ 932.7 eV), Cu(II) ($2p_{3/2}$ 933.7 eV) with an atomic ratio Cu(0)/Cu(II) = 2.6, K (2p 293.3 eV), N (1s 398.3 eV). The observed large C peak is again of the adventitious type (probably due to oil from the diffusion pumps) and cannot be confidently assigned to a specific type of incorporated species. Nevertheless the presence of N and K, which could not be detected on the surface of the sample, can be explained with the incorporation of ionic cyanide-containing species with the respective counter-cations.

3.4. Crystallographic identification of the NS

The NS can be identified as hexagonal with lattice constants: $a = 9.93$ Å, $c = 7.10$ Å. At this stage of our investigation an accurate compositional analysis of the NS was not carried out and structural refinement is consequently not feasible. Inspection of the systematic absences in all diffractograms of electrodeposits obtained on different substrates (X-ray amorphous NiP, annealed Cu, laminated Cu, annealed Ni) shows that both the following conditions are fulfilled:

$$hh(-2h)1 : 1 = 2n \quad (1)$$

$$h(-h)01 : 1 = 2n \quad (2)$$

It should be noted that conditions (1) and (2), limiting possible reflections, are not related to special positions in the space group, but are rather restrictions imposed by the space group. Condition (1) imposes the presence of an *axial glide plane c*, constructed by a mirror operation on a reflection plane with $1(-1)00$ orientation followed by a $c/2$ translation along the z-axis. Condition (2) imposes the presence of an *axial glide plane c*, constructed by a mirror operation on a reflection plane with $11(-2)0$ orientation followed by a $c/2$ translation along the z-axis.

Since some elements of the space-group (e.g., rotation axes, mirror planes) are not directly observable by RDX, the available data allow only the definition of an "extinction symbol" P.cc. This allows the assignment of the NS to one of the two following space groups: 184 (p6cc) or 192 (p6/mcc). On the basis of typical literature values for the c/a ratio, the most probable between these two space groups is 184. As a matter of fact a/c values in the range 7.1–9.8 are very common for the space group 184, while they are very rare for the space group 192. The assignment of the NS to the mentioned symmetry operations corresponds structurally to the repetition with symmetry p6cc (or p6/mcc) of a given group of atoms on planes orthogonal to the z axis and mutually spaced by $c/2$. The analysed structure therefore reasonably consists of a stratification with p6cc (or p6/mcc) symmetry of a system of Au, C, N and K atoms with distances 3.55 Å along the z direction.

This tentative interpretation of a structure electrodeposited in a cyanide environment under conditions of extremely slow growth interestingly recalls structural studies on adsorbed cyanide layers at Pt electrodes. Structural (LEEDS) and compositional (AES) work on CN-overlayers formed on Pt under aqueous electrochemical conditions was carried cut by [8, 9]. It was shown that a monolayer containing C-bound CNH and CN^{-} with associated countercations forms. Countercation exchange in aqueous solutions of different electrolyte composition was proved possible. Highly ordered CN^{-}/CNH mixed monolayers were shown to form. The structure of a CN^{-} layer adsorbed on a Pt(111) electrode was investigated by *in situ* STM in the potential range $-0.5 \div 0$ V (Ag/AgCl) [10] a coverage degree of 7/12 was assessed, the proposed structure features one CN^{-} ion adsorbed on a surface site, at the centre of a hexagonal cluster, the six surrounding adsorbed ions occupying near-surface positions.

3.5. Complementary analyses

3.5.1. RHM

Some mechanical properties of the thin layers deposited under several conditions were estimated by RHM adopting an indented-volume approximation for the evaluation of the thin overlayer contribution to the overall plastic behaviour of the film-substrate system [11]. Thickness was estimated from unitary current efficiency for pure Au electrodeposition. The results for Vickers hardness, Young modulus and plasticity parameter $\delta = \varepsilon_{el}/(\varepsilon_{el} + \varepsilon_{pl})$ are summarised in Table III. The figures reported in this table have a limited quantitative value, owing to the approximation adopted in the data-treatment procedure, nevertheless they allow an accurate ranking of the mechanical properties.

TABLE III Vickers hardness HV (N mm^{-2}), Young modulus Y (GPa) and plasticity parameter δ (%) for thin layers deposited under several conditions. Annealed Cu substrate

	Structure	HV (N mm^{-2})	Y (GPa)	δ (%)
Cu substrate	fcc Cu	83.2	43.5	14.2
Tl^+ 40 ppm, 125 μA cm^{-2}, 2′	Mainly NS	26.2	10.5	30.3
Cu^{2+} 2.5 g l^{-1} 250 μA cm^{-2}, 2′	Mainly NS	23.4	10.8	27.1
Cu^{2+} 2.5 g l^{-1} 250 μA cm^{-2}, 10′	Au + NS	42.7	12.7	19.4
Cu^{2+} 2.5 g l^{-1} 1 mA cm^{-2}, 3′	Mainly Au	58.1	37.7	10.7

3.5.2. Electrical conductivity

In order to gain deeper insight into the structure of these films, electrical conductivity measurements were carried out for samples of similar thicknesses (about 0.75 μm) containing: (i) mainly NS, (ii) a mixture of similar amounts of fcc Au and NS and (iii) mainly fcc Au. Of course in these conditions the penetration depth of the electric field is much higher than the sample thickness (around 400 μm) and quantitative work is not feasible. Nevertheless significant differences (always in excess of 30 standard deviations σ) were measured with respect to the conductivity of the substrate (annealed Cu) and a reliable ranking of the materials can be proposed. The conductivity values clearly group into two classes: samples whose structure is mainly NS show much lower conductivities (85–100 σ) with respect to the Cu substrate than those in which fcc Au is present (30–50 σ). This conclusion is in accord with diffractometric and XPS results implying that the NS most probably contains incorporated extraneous material.

3.6. Electrochemical behaviour

Cathodes immersed in acidic baths containing $KAu(CN)_2$ are strongly passivated [6, 12–15]. This phenomenon has been explained with the presence of surface species containing CN^-, the nature of these species as a function of electrodic potential have been recently studied by *in situ* confocal Raman spectroscopy [14]. These cathodic passivation effects are in part reduced by adding oxidising agents able to scavenge CN^- from the surface, such as H_2O_2. *In situ* Raman spectroscopy was used to assess the effects of the addition of H_2O_2 to the bath in the course of the electrodeposition process. Fig. 12a refers to an electrodeposition process carried out with the bath not containing additives polarised at −400 mV vs. Ag/AgCl, the spectrum displays ν(CN) stretching bands related to: (A) CN^- adsorbed onto metallic Au and (B) adsorbed $Au(CN)_2^-$. After addition of H_2O_2 under the same operating conditions (Fig. 12b) the band (A) is suppressed, the intensity of the band (B) is markedly reduced and band (C), due to formation of CNO^-, appears. In presence of metals giving rise to UPD on Au, depolarisation of the baths can be noticed. Similar effects have been reported previously for Au [12, 15]. In particular, we observed that: (i) for a cathodic voltage ca. equal to the UPD voltage deposition of unalloyed Au is observed, (ii) for voltages more cathodic than the UPD

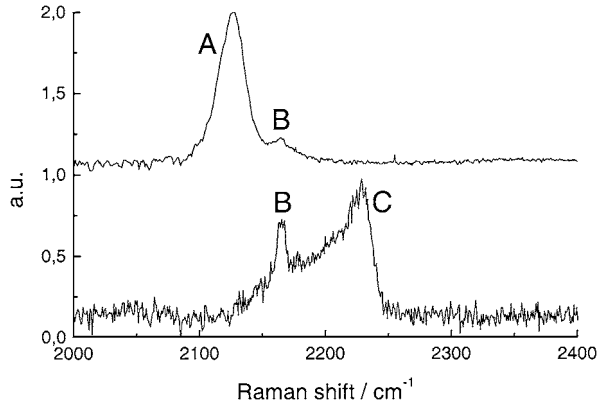

Figure 12 In situ surface Raman spectra obtained during electrodeposition from the $KAu(CN)_2$ bath without additives polarised at −400 mV vs. Ag/AgCl without (a) and with (b) addition of H_2O_2. ν(CN) stretching bands of: (A) CN^- adsorbed onto metallic Au, (B) $Au(CN)_2^-$, (C) CNO^-.

voltage, some metals give rise to alloying according to mechanism which still need to be deepened (e.g., codeposition of equiatomic AuCu) while other metals do not codeposit (e.g., Tl). The UPD deposition of Cu^{2+} on polycrystalline Au was studied in 0.5 M Na_2SO_4 at pH 3; UPD parameters $\Delta E_p = 220$ mV and $d_{1/2}$ 110 mV were measured [16]. More extensive investigations were recently carried out on the Au (111) surface in H_2SO_4, showing two well defined peaks, which have been related to a 2D structure [17–21]. These two peaks were interpreted in terms of 1 and 2 electron transfer mechanisms, respectively. For a range of operating conditions typical parameters of these two peaks are: $\Delta E_p(1) = 20$–50 mV, $d_{1/2}(1) = 15$–35 mV; $\Delta E_p(2) = 215$ mV, $d_{1/2}(2) = 5.0$–15 mV. The variation of peak positions was measured as a function of $[Cu^{2+}]$, which linearly shifts the couples of peaks (more anodic UPD features were observed for lower $[Cu^{2+}]$) [22] Effects of coadsorption of SO_4^{2-}, Cl^- and Br^- on UPD of Cu onto Au (111) were studied in [23], significant shifts of the peak positions and intensities were observed: the halides tend to shift the first one to more cathodic values and the second one to more anodic potentials.

The UPD deposition of Tl^+ on polycrystalline Au was studied in 0.5 M Na_2SO_4 at pH 3); UPD parameters $\Delta E_p = 690$ mV and $d_{1/2}$ 120 mV were measured [16, 24–26]. Analyses of UPD Tl stripping peaks from Au (111), (100), (110) were performed [27]. It was observed that the Nernstian potential of the Tl/Tl^+ couple is more negative than the hydrogen evolution potential, nevertheless hydrogen evolution is strongly inhibited by the underpotential adsorption of Tl. One stripping peak was observed with (111) at $\Delta E_p = +400$ mV $d_{1/2} = 21$ mV, two peaks were observed with (100) at +85 ($d = 100$) and +235 ($d = 22$) mV and two poorly defined peaks at ∼+100 and at ∼+700 on (110). Two pronounced peaks were measured at −400 and −450 mV vs. SCE on Au (111) in 0.1 M $HClO_4$ [28]. [12, 13] studied polycrystalline Au surfaces in 0.1 M KOH. The OPD peak of Tl (0.1 mM) was measured at −0.57 V vs. SHE, while the UPD peak of Tl was recorded at −0.1V vs. SHE, notwithstanding the peak position, UPD is reported to occur up to 0.2 V. The stripping curve displays an oxidation peak

of hydrated Tl_2O_3 at 0.15 V, anhydrous Tl_2O_3 is subsequently formed at 0.29 V vs. SHE, Addition of KCN brings about a significant increase of the rate of Au dissolution in the range of Tl UPD (−0.6–0.2 V vs. SHE); reduction of $Au(CN)_2^-$ formed anodically is observed at −0.5 V vs. SHE. If $KAu(CN)_2$ is added $Au(CN)_2^-$ reduction processes are observed below ∼−300 mV vs. SHE on negative scans following the first one (on the first one CN^- is produced at the electrode surface). In the absence of Tl^+, $Au(CN)_2^-$ reduction is inhibited from the start of this process to ∼−700 mV vs. SHE: a small pre-wave was noticed and attributed to the reduction of CN^- containing oxide film [29] or AuCN films [15]. In the presence of Tl^+ the rate of $Au(CN)_2^-$ reduction is considerably increased in the potential region of the pre-wave and the main peak of $Au(CN)_2^-$ reduction is shifted in the anodic direction by $\sim 200 \div 400$ mV, as a function of $[Tl^+]$ and $[Au(CN)_2^-]$. On the positive sweep significant Au dissolution is observed in the potential range −600 to −200 mV vs. SHE, due to free cyanide ions at the electrode surface produced in the negative scan and the strong catalytic effect of Tl^+ both on $Au(CN)_2^-$ reduction and on Au dissolution.

The CV for the polycrystalline Au electrode in the citrate supporting electrolyte is reported in Fig. 13. Hydrogen evolution is observed for cathodic voltages past a value which is very close to the Nernstian one for the given pH. $Au(CN)_2^-$ reduction is observed at ∼−550 mV vs. SCE. This potential is very removed from typical equilibrium ones for near neutral solutions reported in [15, 30], the immersion potential value for the $Au/Au(CN)_2^-$ couple is severely affected by adsorbed CN^-, which is known to be a very complex process with hysteretic behaviour and sluggish kinetics [14]. The distinct pre-wave reported in alkaline solutions [12] could not be observed. Nevertheless c.d.s in the range $-700 \div -900$ mV vs. SCE are slightly higher than for supporting electrolyte, which, in accord with [30] is indicative of simultaneous hydrogen evolution and Au reduction.

The CV for Tl^+ on Au is reported in Fig. 14. Two Tl UPD features are observed in the cathodic scan at ∼−660 and −900 mV vs. SCE. Tl OPD starts for $V < -1000$ mV vs. SCE in this environment. Two Tl stripping peaks are noticed at ∼−750 and −570 mV vs. SCE. A similar behaviour was reported for different

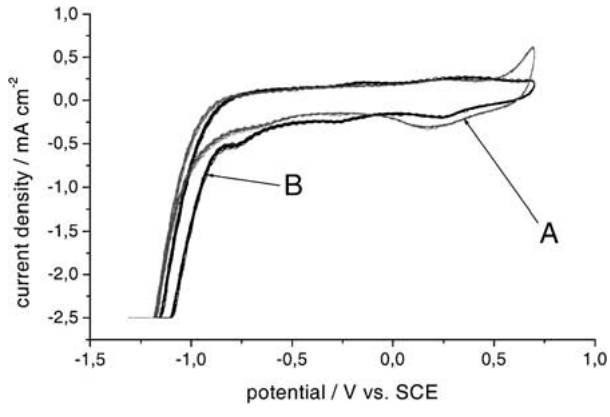

Figure 13 Cyclic voltammograms for polycrystalline Au electrode in the citrate supporting electrolyte without (A) and with (B) 0.6 g l^{-1} $KAu(CN)_2$.

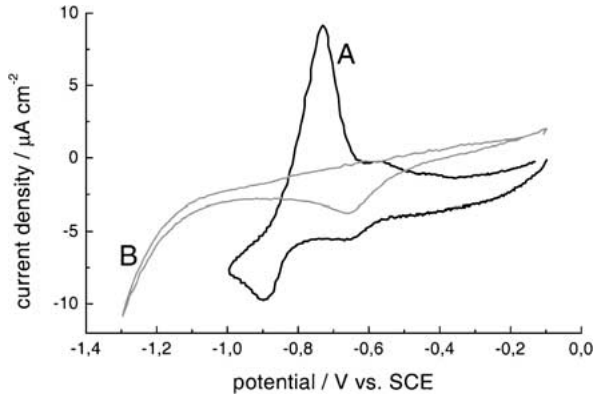

Figure 14 Cyclic voltammograms for polycrystalline Au electrode in the citrate supporting electrolyte containing 40 ppm Tl^+ without (A) and with (B) 0.6 g l^{-1} $KAu(CN)_2$.

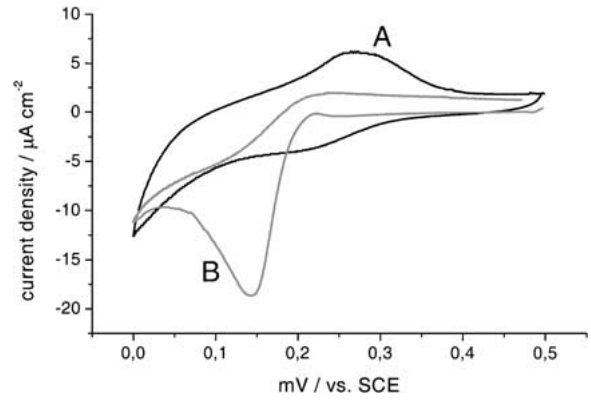

Figure 15 Cyclic voltammograms for polycrystalline Au electrode in the citrate supporting electrolyte containing 125 ppm Cu^{2+} without (A) and with (B) 0.6 g l^{-1} $KAu(CN)_2$.

electrolytes: [15] for a phosphate buffer at pH 8, [12] for 0.1 M KOH. The CV for $Au(CN)_2^-$ and Tl^+ is also shown. A significant cathodic depolarisation is noticed, the cathodic process starts at ∼−400 mV vs. SCE and a stripping peak could not be observed. The depolarising action was observed in [15] and explained with an exchange reaction, but the CV behaviour was not reported in phosphate buffer at pH 8 and no information is available on the stripping behaviour of Tl during Au codeposition. The disappearance of the stripping peak, together with the observation that no observable amounts of Tl can be detected in Au electrodeposits from Tl-containing baths supports the exchange depolarisation mechanism proposed in [15]. In [12] CVs in 0.1 M KOH were reported, but a Tl stripping peak could be observed.

The CV for Cu^{2+} is shown in Fig. 15. Cu UPD and stripping peaks can be noticed at ∼+200 mV vs. SCE and at +270 mV vs. SCE, respectively. Similar observations were reported e.g., in [31]. The CV for Cu^{2+} and $Au(CN)_2^-$ is also reported. The UPD peak is enhanced and shifted to more cathodic values (∼150 mV vs. SCE) by the presence of $Au(CN)_2^-$ while the stripping peak disappears. The disappearance of the stripping peak, together with the observation of a stoichiometric 50 at.% AuCu composition of the deposits seems to suggest the UPD of Cu depolarises Au deposition and gives rise to the formation of an alloy in which Cu is markedly more noble than UPD Cu on Au.

(i) In solutions containing only Au(I) ions and a polycrystalline Au electrode, the polarisation of the bath during the cathodic scan is confirmed. In the anodic scan oxide formation can be observed. (ii) In solutions containing only Cu^{2+} or Tl^{+} UPD of these metals on polycrystalline Au is observed in the cathodic scan and stripping in the anodic scan. (iii) In solutions containing both Au(I) ions and Cu^{2+} or Tl^{+}, Au electrodeposition is observed during the cathodic scan at exactly the same potentials as the UPD ones. No stripping peaks can be observed in the anodic scan in this system.

These results can be interpreted under the hypothesis that if inhibition by CN^{-}-containing species is present, the metals giving rise to UPD on Au can promote the assisted Au deposition according to the following mechanism:

(i) UPD of Me^{z+} onto a fraction of the cathodic surface via one of the following possible mechanisms: (a) infiltration of the adsorbed CN^{-} layer; (b) substitution through competition with species giving rise to the inhibition of Au deposition on Au; (c) reductive adsorption of Me^{z+} onto the CN^{-} layer. Step (i) is, notwithstanding the exact nature of the reduction mechanism (a–c), in accord with the phenomena described in [12] where a reduction of interfacial CN^{-} concentration is reported in presence of metallic species giving rise to UPD effects onto Au.

(ii) Displacement of the Me adlayer via oxidation by Au(I).

(iii) Iteration of the competitive inhibition and reactivation processes on the Au(0) layer, giving rise to a cyclic mechanism.

At present it is not possible to provide detailed information on the alternative reduction mechanisms (i.a–c); in any case the hypotheses to be proposed will have to take into account the presence of hexagonal structures containing Au and CN groups highlighted in this work.

4. Conclusions

Au electrodeposition at current density <0.25 mA cm^{-2} from dicyanoaurate baths with or without Cu^{2+} or Tl^{+}, gives rise to the formation of a hexagonal structure not previously reported. Such structure displays a large unit cell, probably due to the incorporation of cyanide-related species. XPS spectra from the bulk of the deposit reveal the presence of sizeable amounts of C, N and K. On the basis of the available structural and compositional data, the new hexagonal structure can be assigned to the space group 184 (p6cc). The new structure is typically part of a two-phase system also containing fcc Au; the content of the former phase is enhanced by lower current densities, short deposition times and addition of metal ions displaying UPD behaviour on Au.

Preliminary data on the mechanical and electrical properties of the new phase were obtained by microindentation and electrical conductivity measurements. The new phase has poorer mechanical properties than fcc Au: lower hardness, lower Young modulus and lower plasticity. The electrical conductivity of this phase is markedly lower than that of the codeposited fcc Au. Mechanical and electrical data support the view that this hexagonal phase is partly non metallic in nature.

As far as the electrokinetic behaviour of this system is concerned, cyanoaurate baths display cathodic passivation linked to the release of free CN^{-} at the electrode intrerface. The cathodic inhibition is reduced by addition of metal cations giving rise to UPD, such as Cu^{2+} and Tl^{+}. Codeposition of Au from $Au(CN)_2^{-}$ and Tl or Cu gives rise to species which are more anodically stable than the single metals, and no stripping peaks appear in the anodic scan of the relevant cyclic voltammograms. This phenomenology is probably related to the cathodic interaction of the codepositing metals giving rise to an enhancement of Au(I) reduction linked to oxidative desorption of UPD Tl and surface alloying with UPD Cu.

References

1. E. RAUB and F. SAUTTER, *Metalloberfläche* **10** (1956) 65.
2. S. STEINMANN, W. FLÜMANN and W. SAXER, *ibid.* **29** (1975) 154.
3. F. SIMON, *Gold Technology* **16** (1995) 22.
4. B. BOZZINI, G. GIOVANNELLI and P. L. CAVALLOTTI, *J. Appl. Electrochem.* **29** (1999) 685.
5. B. BOZZINI, G. GIOVANNELLI, S. NATALI, B. BREVAGLIERI, P. L. CAVALLOTTI and G. SIGNORELLI, *Eng. Fail. Anal.* **6** (1999) 83.
6. B. BOZZINI, P. L. CAVALLOTTI, G. GIOVANNELLI and S. NATALI, in Proc. 197th ECS Meeting, Toronto, Canada, 14–18 May, 2000, PV 2000–16 Electrochemical Society Proceedings, edited by G. Jerkiewicz, J. M. Feliu and B. N. Popov (Electrochemical Society, Pennington, N J, USA) p. 242.
7. B. BOZZINI, G. GIOVANNELLI and S. NATALI, *Scripta Materialia* **43** (2000) 877.
8. S. D. ROSASCO, J. L. STICKNEY, G. N. SALAITA, D. G. FRANK, J. Y. KATEKARU, B. C. SCHARDT, M. P. SORIAGA, D. A. STERN and A. T. HUBBARD, *J. Electroanal. Chem.* **188** (1985) 95.
9. B. C. SCHARDT, J. L. STICKNEY, D. A. STERN, D. G. FRANK, J. Y. KATEKARU, S. D. ROSASCO, G. N. SALAITA, M. P. SORIAGA and A. HUBBARD, *Inorg. Chem.* **24** (1985) 1419.
10. C. STUHLMANN, I. VILLEGAS and M. J. WEAVER. *Chem. Phys. Lett.* **219** (1994) 319.
11. B. BOZZINI, P. L. CAVALLOTTI, M. BALBI and M. BONIARDI, *Met. Ital.* **90** (1998) 23.
12. D. POSKUS, G. AGAFONOVAS and I. JURGAITIENE, *J. Electroanal. Chem.* **425** (1997) 107.
13. D. POSKUS and G. AGAFONOVAS, *ibid.* **493** (2000) 50.
14. B. BOZZINI, G. GIOVANNELLI, C. LENARDI, C. MELE and M. SERRA. in Proc. ECS Spring Meeting, Washington DC, in press.
15. J. D. E. MCINTYRE and W. F. PECK, *J. Electrochem. Soc.* **123** (1976) 1800.
16. D. M. KOLB, M. PRZASNYSKI and H. GERISCHER, *J. Electroanal. Chem.* **54** (1974) 25.
17. D. M. KOLB, *Ber. Bunsenges. Phys. Chem.* **92** (1988) 1175.
18. A. ABERDAM, R. DURAND and R. FAURE, *J. Chim. Phys.* **88** (1991) 1519.
19. N. BATINA, T. WILL and D. M. KOLB, *Faraday Disc.* **94** (1992) 93.
20. O. MAGNUSSEN, J. HOTLOS, R. NICHOLS and D. KOLB, *R. Behm. Phys. Rev. Lett.* **64** (1990) 2929.
21. J. G. GORDON, O. R. MELROY and M. F. TONEY, *Electrochim. Acta* **40** (1995) 3.
22. I. OMAR, H. PAULING and K. JÜTTNER, *J. Electrochem. Soc.* **140** (1993) 2187.
23. Z. SHI, S. WU and J. LIPKOWSKI, *Electrochim. Acta* **40** (1995) 9.

24. E. SCHMIDT, N. WÜTHRICH, *J. Electroanal. Chem.* **34** (1972) 377.
25. V. A. VICENTE and S. BRUCKENSTEIN, *Anal. Chem.* **45** (1973) 2036.
26. G. SALIÉ and K. BARTELS, *Electrochim. Acta* **39** (1994) 1057.
27. J. W. SCHULTZE and D. DICKERTMANN, *Surf. Sci.* **54** (1976) 489.
28. R. R. ADZIC, J. WANG and B. M. OCKO, *Electrochim. Acta* **40** (1995) 83.
29. I. R. BURROWS, J. A. HARRISON and J. THOMPSON, *J. Electroanal. Chem.* **35** (1974) 283.
30. H. Y. CHEH and R. SARD, *ibid.* **116** (1971) 1737.
31. C. ALONSO, A. B. SALOMÓN and H. D. ABRUÑA, *Z. für Phys. Chem.* **210** (1999) 15.

Received 21 August 2001
and accepted 15 May 2002